NANO LETTERS

Letter

pubs.acs.org/NanoLett

Sequence of Silicon Monolayer Structures Grown on a Ru Surface: from a Herringbone Structure to Silicene

Li Huang,[†,§] Yan-Fang Zhang,[†,∥] Yu-Yang Zhang,[‡,∥] Wenyan Xu,[†] Yande Que,[†] En Li,[†] Jin-Bo Pan,[†] Ye-Liang Wang,[†,‡] Yunqi Liu,[§] Shi-Xuan Du,*[,†,‡] Sokrates T. Pantelides,*[,∥,‡] and Hong-Jun Gao*[,†,‡]

[†]Institute of Physics, Beijing Key Laboratory for Nanomaterials and Nanodevices, Chinese Academy of Sciences, Beijing 100190, P. R. China

[‡]School of Physical Sciences and CAS Key Laboratory of Vacuum Physics, University of Chinese Academy of Sciences, Beijing 100049, P. R. China

[§]Institute of Chemistry, Chinese Academy of Sciences, Beijing 100190, P. R. China

[∥]Department of Physics and Astronomy and Department of Electrical Engineering and Computer Science, Vanderbilt University, Nashville, Tennessee 37235, United State

S *Supporting Information*

ABSTRACT: Silicon-based two-dimensional (2D) materials are uniquely suited for integration in Si-based electronics. Silicene, an analogue of graphene, was recently fabricated on several substrates and was used to make a field-effect transistor. Here, we report that when Ru(0001) is used as a substrate, a range of distinct monolayer silicon structures forms, evolving toward silicene with increasing Si coverage. Low Si coverage produces a herringbone structure, a hitherto undiscovered 2D phase of silicon. With increasing Si coverage, herringbone elbows evolve into silicene-like honeycomb stripes under tension, resulting in a herringbone-honeycomb 2D superlattice. At even higher coverage, the honeycomb stripes widen and merge coherently to form silicene in registry with the substrate. Scanning tunneling microscopy (STM) was used to image the structures. The structural stability and electronic properties of the Si 2D structures, the interaction between the Si 2D structures and the Ru substrate, and the evolution of the distinct monolayer Si structures were elucidated by density functional theory (DFT) calculations. This work paves the way for further investigations of monolayer Si structures, the corresponding growth mechanisms, and possible functionalization by impurities.

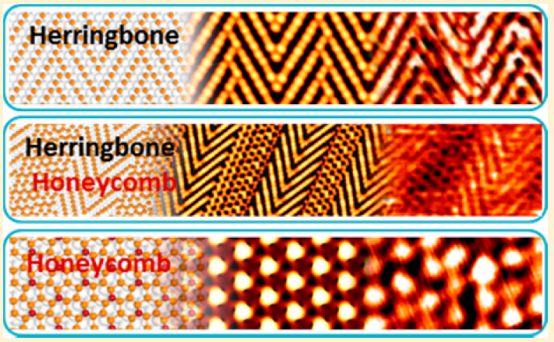

Two-dimensional materials have generated growing interest because of the possibility that they can be used to fabricate ultrathin, high-quality, semiconductor layers with high carrier mobility.[1−4] Silicene, a one-atom-thick crystal composed of Si atoms with a buckled honeycomb lattice structure, has been fabricated and investigated in order to explore its properties and its potential for applications in Si-based devices.[5−15] A substantial number of investigations, both experimental and theoretical, focus mainly on silicene superstructures grown on Ag(111) substrates.[9,16−19] However, the interaction between silicene and silver substrate is relatively strong. Recently, quasi-freestanding epitaxial silicene was achieved on a Ag(111) substrate by using oxygen intercalation, which may increase the likelihood of applications.[20] A few reports have shown that silicene can be grown on other substrates, such as Ir(111),[10] ZrC(111),[12] and ZrB_2(0001),[21] but the coupling between silicene and these substrates is strong. In order to look for a suitable substrate that has weak interactions with the silicene layer and improve the sample quality, it is useful to understand the growth process of silicene.

The Ru(0001) surface has been used extensively as a substrate for graphene growth because it yields exceptionally high-quality material.[22−24] In this letter, we used a Ru(0001) substrate to grow silicon monolayers. In the process we discovered a number of distinct Si monolayer structures, some of which have not been discovered before, with the final product being high-quality silicene. At low coverage, Si atoms occupy substrate 3-fold hollow sites and form a herringbone monolayer structure. With increasing Si coverage, the new Si atoms adsorb around herringbone elbows, forming the first hexagons for the nucleation of silicene growth. As additional Si atoms arrive, the initial hexagons at herringbone elbows develop into small honeycomb patches, which then evolve into long, narrow, silicene ribbons in tension, resulting in alternating herringbone and silicene nanoribbons. As Si coverage is increased further, the long silicene ribbons merge

Received: November 17, 2016
Revised: January 18, 2017
Published: January 18, 2017

DOI: 10.1021/acs.nanolett.6b04804
Nano Lett. 2017, 17, 1161−1166

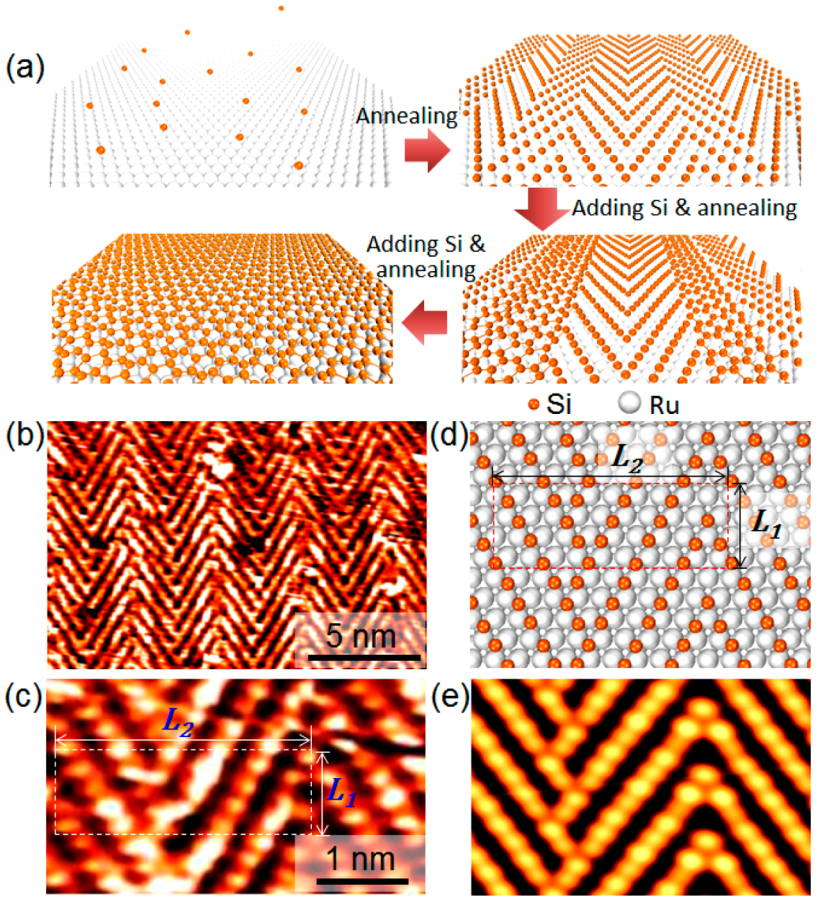

Figure 1. Experimental process and the Si herringbone structure on a Ru(0001) substrate. (a) Experimental process of Si monolayer structures formed on Ru(0001) (Si and Ru atoms are represented by orange and silver balls, respectively). (b) Large-area STM image of Si herringbones (−0.10 V, 1.52 nA). (c) Atomic-resolution STM image (−0.13 V, 2.94 nA). The unit cell is outlined by a white rectangle. The vertical distance between two neighboring elbows is L_1. The periodicity along a single herringbone chain is L_2. (d) Atomic model of the Si herringbone structure. The unit cell is outlined by a red rectangle. (e) Simulated STM image of a Si herringbone structure.

into silicene sheets, while the herringbones vanish. The net result is the formation of a buckled silicene on a Ru(0001) substrate. The silicene grows in one of two possible orientations with a 22° rotation angle, which is imposed by the substrate.

Figure 1a shows the experimental process schematically. In order to explore the evolution from the initial stage, a small amount of Si atoms were deposited on a Ru(0001) substrate (the first step in Figure 1a) using MBE (see Methods). It is worth noting that we found a large area of a hitherto undiscovered substrate-supported Si herringbone-structure monolayer forms after annealing the sample at 500 °C, as shown in Figure 1b. The Si herringbone structure has an angle of 60° at the elbows. Figure 1c is an atomic-resolution STM image of Si herringbones. The vertical distance between two adjacent elbows in neighboring herringbone chains, L_1, is ∼9 Å, and the distance between two adjacent elbows along the same herringbone chain, L_2, is around 30 Å (see Figure 1c).

A theoretical model (Figure 1d) of the observed herringbone structure has been constructed based on the STM images. In the model, there are 11 Si atoms on each ridge, i.e. along the $[2\bar{1}\bar{1}0]$ and $[\bar{1}\bar{1}20]$ directions of the Ru(0001) substrate. The simulated STM image, shown in Figure 1e, is in good agreement with the atomic-resolution STM image in Figure 1c. The formation of the herringbone structure can be explained as follows. Whereas an isolated Si atom binds at a hexagonal-close-packed (HCP) hollow site with a binding energy of 4.95 eV, forming Si chains by occupying neighboring HCP hollow sites increases the binding to 5.41 eV/Si atom. The 3-fold symmetry of the substrate further leads to parallel chains at 60° angles, which then leads to herringbone structures, increasing the binding to 5.42 eV/Si atom. Compared with parallel monatomic chains, the herringbone structure is energetically more stable, resulting in Ru atoms under herringbone ridges bonding to two Si atoms, while those near each apex bond to one. Binding energy per Si atom in different Si structures on Ru substrate confirms that Si herringbone structure is the most stable structure at low Si coverage (Table S1 and Figure S1).

Figure 2a shows that despite the large bond length (2.73 Å in average), there is substantial electron density between Si atoms. (In Supporting Information, Figure S2a, we show that binding in a free Si dimer remains substantial even at relatively larger separations.) Overall, the formation of herringbones represents a significant low energy compared with random binding of Si atoms on HCP hollow sites (5.42 eV/Si atom versus 4.95 eV for isolated Si atoms).

We checked the structural stability of the epitaxial herringbone structure by calculating the phonon spectra (see Figure S2b). Though there are strong interactions between Si atoms and Ru substrate (reflecting by a substantial electron density between Si and Ru atoms in Figure 2b), there are no

DOI: 10.1021/acs.nanolett.6b04804
Nano Lett. 2017, 17, 1161−1166

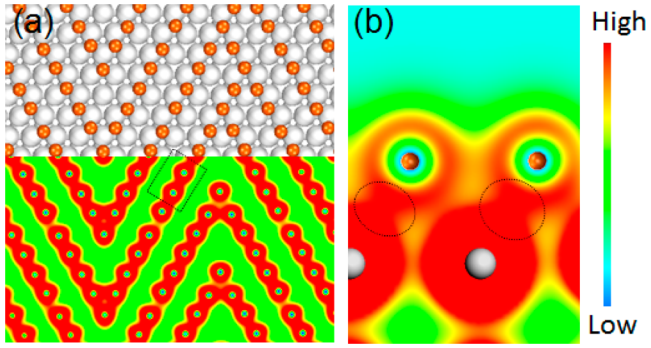

Figure 2. Electron density of Si herringbones on Ru(0001). (a) Geometric structure and electron density of Si herringbones on Ru(0001). The dashed black rectangle shows substantial electron density between Si atoms indicating interatomic interaction. Electron density of Ru atoms is hidden. (b) Side view of electron density distribution. The dashed black circles show substantial electron density between Si and Ru atoms.

negative-frequency modes, which is an indication of stability.[25] The large bond lengths and low atom density suggest that the herringbone structure would not hold up as a free-standing monolayer, but its stability on the Ru substrate suggests that it can potentially serve as a template for functionalization by impurities and other means. Energy bands for a hypothetical free-standing herringbone structure are shown in Figure S3a. The corresponding energy bands for epitaxial herringbone structure are shown in Figure S3b. Both show metallic behavior with no Dirac cone.

With further increase of Si coverage, the STM data reveal that the herringbone elbows evolve into honeycomb hexagons and give rise to honeycomb stripes that alternate with the herringbone remnants, i.e., a herringbone-honeycomb 2D superlattice, as shown in Figure 3a. The superlattice can grow in different orientations with an angle of 60°, determined by the 3-fold symmetric substrate. The honeycomb stripes are in tension and the honeycomb hexagons are distorted. The widths of the herringbone stripes in the superlattice range from 24 to 28 Å while the widths of the honeycomb stripes range from 9 to 27 Å. The adsorbates (bright protrusions in Figure 3a) are likely to be stray Si atoms because they only appear when the surface is covered with the herringbone-honeycomb 2D superlattice. Figure 3b shows a schematic model of the herringbone-honeycomb 2D superlattice. Zoom-in STM images of the herringbone−honeycomb 2D superlattice and hexagons in the honeycomb structure are presented in Figures 3c and 3d, respectively.

We have performed calculations to elucidate the evolution of the herringbone structure into a herringbone-honeycomb 2D superlattice, which can also be viewed as the nucleation and growth of honeycomb stripes that ultimately evolve into large-area silicene (see below). As shown in Figure 1, there are extra Si atoms around Si herringbone elbows, which indicate that excess Si atoms are more likely to adsorb at elbows. By comparing calculated binding energies, we find that site 1 and site 2 (see Figure 4a) are the most stable adsorption sites for an extra Si atom. A hexagon forms when both site 1 and site 2 are occupied by Si atoms. Clearly, the hexagon acts as a nucleation site for the growth of silicene-like honeycomb structures.

An *ab initio* molecular dynamics (MD) simulation was performed based on this model to further elucidate the honeycomb nucleation process. Our purpose was to observe and study the transition from herringbone to honeycomb structure. Nine more Si atoms were added around the elbow as shown in Figure 4b, and the system was simulated at 400 K for 5 ps. A typical snapshot after reaching equilibrium is shown in Figure 4c, in which we can see clearly the formation of a distorted silicene-like honeycomb stripe. This simulation demonstrates that the honeycomb stripes in the herringbone−honeycomb 2D superlattice seen in the experimental data grow from the elbows of herringbones. In addition, the statistics of Si−Si distances in one of the honeycomb hexagons are shown in Figure S4 as a function of simulation time. They confirm that the hexagons are distorted and the silicene-like honeycomb stripes are in tension.

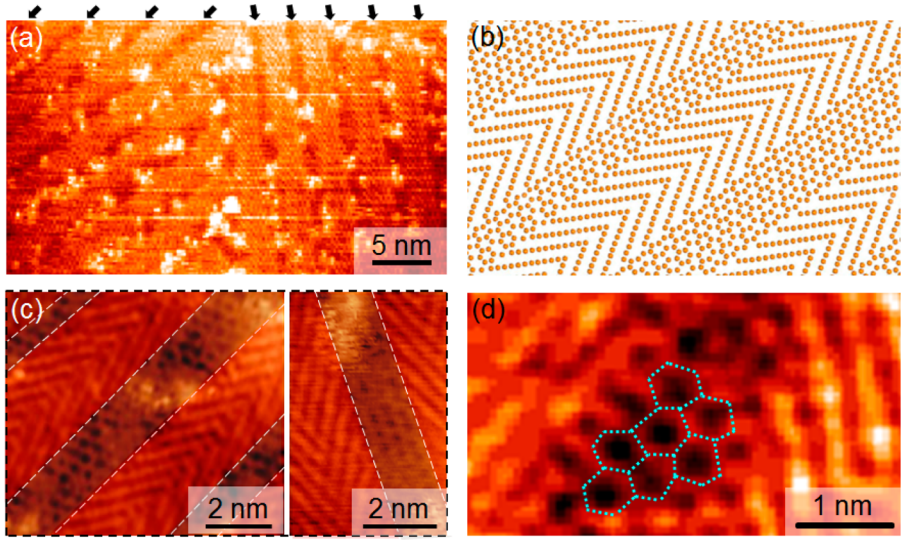

Figure 3. Herringbone-honeycomb superlattice. (a) Large-area STM image of the herringbone-honeycomb 2D superlattice (−0.86 V, 0.22 nA). The short black arrows on top of the figure are used to demarcate the honeycomb stripes in the superlattice. (b) Schematic model of a herringbone-honeycomb 2D superlattice. (c) Zoom-in STM image, where the honeycomb stripes are marked in red-brown and the herringbones in gray-brown. (d) High resolution STM image shows details of the distorted hexagons (−3.8 V, 0.38 nA).

DOI: 10.1021/acs.nanolett.6b04804
Nano Lett. 2017, 17, 1161−1166

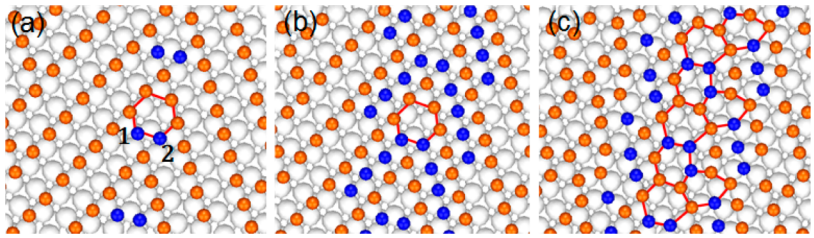

Figure 4. Schematic of the nucleation site for silicene-like honeycomb growth. (a) Herringbone structure with extra silicon atoms (blue balls) at elbows. Orange balls indicate Si atoms in herringbones. Sites 1 and 2 are two HCP hollow sites that, when occupied by Si atoms, complete a hexagon (marked by red lines). (b) Initial herringbone structure with more extra Si atoms (in blue) for a MD simulation. (c) Snapshot from MD simulation shows formation of distorted honeycomb hexagons (distorted silicene).

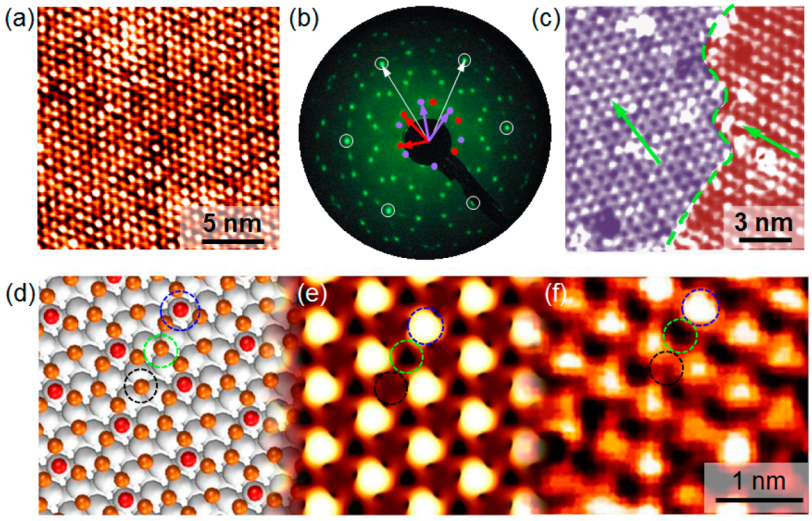

Figure 5. STM, LEED pattern, and atomic model of the silicene layer on Ru(0001). (a) STM image, showing a $(\sqrt{7} \times \sqrt{7})$ superstructure of a silicene layer on Ru(0001) (−1.32 V, 0.11 nA). (b) LEED pattern of a Si monolayer on Ru(0001). The spots marked by white circles are from Ru(0001); other spots are from silicene. (c) STM image of two equivalent domains of the $(\sqrt{7} \times \sqrt{7})$ superstructure (−0.85 V, 0.11 nA). The two domains are colored in purple and red. The green dashed line marks the domain boundary; the two green arrows indicate the high symmetric directions of the two domains. (d) Top view of the optimized atomic model. (e) Simulated STM image. Three distinct regions are identified by circles and discussed in main text. (f) High-resolution STM image (−0.85 V, 0.11 nA).

With a further increase of Si coverage, the STM data reveal that the honeycomb stripes in the superlattice grow in width, consume the herringbone stripes, and form a silicene layer on the entire surface. A large-scale STM image is shown in Figure 5a. The periodicity of the bright moiré pattern is 0.72 nm, indicating a $(\sqrt{7} \times \sqrt{7})$ superstructure ($\sqrt{7}$ of the lattice constant of Ru(0001), namely $\sqrt{7} \times 0.271$ nm = 0.72 nm). A low-energy electron diffraction (LEED) pattern is shown in Figure 5b, in which the white circles are contributed by the Ru(0001) substrate and the red/purple dots are contributed by the silicene moiré pattern. There are two sets of spots contributed by the silicene moiré pattern (red and purple dots) indicating two silicene domains, with a rotation angle of 22° (marked by the red and purple arrows). The rotation angle is exactly the angle between two $(\sqrt{7} \times \sqrt{7})$ domains on a Ru(0001) substrate as shown in Figure S5. The boundary between two domains was found and shown in Figure 5c by scanning a large area (the two domains are colored in purple and red). Moreover, the LEED pattern is unchanged over the whole surface, suggesting that the silicene layer covers the entire substrate.

An atomic model of silicene in registry with $(\sqrt{7} \times \sqrt{7})$ Ru(0001) has been constructed based on the LEED pattern and high-resolution STM images. A top view of the fully relaxed structure is shown in Figure 5d. This is buckled silicene. The Si−Si distance varies from 2.38 to 2.86 Å. The Si atoms with the highest elevation from the substrate (red color in Figure 5d), occupy top sites, with a vertical distance of 2.85 Å to the substrate. The rest of the Si atoms (orange color) are 1.26 Å lower in average than the top Si atoms, resulting in silicene with a buckled structure (for comparison, the buckling of free-standing silicene is 0.5 Å). The significantly large buckling distance is also found on other substrates, e.g., 1.2 Å on Ag substrate.[26] The binding energy of silicene on a Ru substrate is 0.97 eV/Si atom, comparable with 0.77 eV/Si atom on a Ag substrate $(\sqrt{7} \times \sqrt{7})$ structure.[26]

Energy bands for a free-standing silicene structure are shown in Figure S6a. The corresponding energy bands for epitaxial silicene structure are shown in Figure S6b. The Dirac cone character of free-standing silicene disappears when silicene forms on a Ru substrate, just as silicene on a Ag substrate.[26] The ultimate goal of preparing free-standing silicene with a Dirac cone is still out of reach.

The simulated STM image, shown in Figure 5e, is in good agreement with the high-resolution STM image of Figure 5f. Parts e and f of Figure 5 show that the STM image of silicene on a Ru substrate contains spots of three different degrees of brightness that we shall call bright, intermediate, and dark spots

DOI: 10.1021/acs.nanolett.6b04804
Nano Lett. 2017, 17, 1161−1166

(marked by the blue, green, and black circle, respectively). The bright spots correspond to the highest Si atoms together with their three neighboring Si atoms. The spots of intermediate brightness correspond to Si atoms at HCP hollow sites, where the electron density is lower than that of the atop Si atoms. The dark spots correspond to Si atoms close to bridge sites, where the electron density is lowest. These facts verify that the model is consistent with what we observe in the experiments. We verified that the observed structure is not a form of Ru silicide by simulating STM images of surfaces of RuSi, Ru_2Si_3 (see Figure S7). They all show significant differences from our experimental data.

During the evolution process of distinct Si monolayer structures, Si atoms bond with Ru substrate strongly at all coverages. The energy gain of the herringbone and silicene structure is 5.42 and 5.39 eV/Si atom, respectively. At low coverage, the herringbone structure forms because it is kinetically possible and thermodynamically favored. Silicene forms at a higher coverage when the herringbone structure is sterically prohibited. At even higher coverage, 3D silicon would form.

In conclusion, a sequence of Si monolayer structures are successively formed during the growth process of silicene on a Ru(0001) substrate, and the evolution process is observed and confirmed by combining STM measurement with DFT calculations. A Si herringbone structure forms at low Si coverage. With increasing Si coverage, the new Si atoms adsorb at elbows of Si herringbones and form hexagons acting as nucleation sites for silicene growth. The hexagons, together with the extra Si atoms, develop into small patches composed of hexagons and then gradually develop into silicene nanoribbons under tension. The buckled silicene layer on Ru(0001) forms with further increasing Si coverage. This work identified distinct Si monolayer structures grown on a Ru(0001) substrate and elucidated the step-by-step growth of silicene. The new structures can lead to additional investigations of Si monolayers, possibly to functionalize them by using either substitutional impurities or adatoms, for quantum computing or other applications.

Methods. The experiments were performed in an ultrahigh vacuum (UHV) system with a base pressure better than 2×10^{-10} mbar. The system is equipped with a scanning tunneling microscope (STM) and a low-energy electron diffraction (LEED) system. The Ru(0001) substrate was sputtered by Ar^+ and then annealed to 1000 °C for several cycles to yield a clean surface, which was confirmed by LEED and STM. The Si atoms were evaporated onto a clean Ru(0001) surface and the sample was annealed to 500 °C before checked by STM at room temperature. Cycles of Si evaporating and annealing of the sample were repeated to obtain higher Si coverage on Ru(0001).

The calculations were carried out with the generalized gradient approximation (GGA)[27] in the Kohn–Sham equations as implemented in Vienna *ab initio* simulation package (VASP).[28] Wave functions were expanded in a plane-wave basis set up to 400 eV energy cutoff. The projected augmented wave (PAW) method was used to describe the core–valence interactions. A slab model is used with four Ru layers as the substrate. The vacuum layer is larger than 15 Å. All atoms except the bottom two Ru layers are fully relaxed until the net force is smaller than 0.01 eV/Å. STM images were simulated based on the Tersoff-Hamann approximation.[29] For *ab initio* molecular dynamics (MD) simulations,[30,31] a canonical (NVT) ensemble was used at 400 K. Time interval between each steps is 1 fs. We checked the existence of negative-frequency phonon modes to test the structural stability.[25,32] The dynamical matrix was calculated with the finite-displacement method, with each displacement at 0.02 Å.[33] The total energy is converged to 10^{-6} eV for the phonon calculations. As the cell is large, only the Γ point is sampled to generate phonon density of states

■ ASSOCIATED CONTENT

Supporting Information

The Supporting Information is available free of charge on the ACS Publications website at DOI: 10.1021/acs.nanolett.6b04804.

Binding energy per Si atom in different Si monolayer structures on Ru(0001) substrate, interatomic energy between two Si atoms in a Si dimer, the stability of Si herringbone on Ru(0001) substrate, the electronic structure of Si herringbones and silicene on Ru(0001) substrate, and the exclusion of several Si–Ru alloy structures (PDF)

■ AUTHOR INFORMATION

Corresponding Authors

*E-mail: hjgao@iphy.ac.cn (H.-J.G.).
*E-mail: pantelides@vanderbilt.edu (S.T.P.).
*E-mail: sxdu@iphy.ac.cn (S.-X.D.).

ORCID

Shi-Xuan Du: 0000-0001-9323-1307

Author Contributions

L.H. and Y.-F.Z. contributed equally to this work.

Notes

The authors declare no competing financial interest.

■ ACKNOWLEDGMENTS

We acknowledge the financial support from National Key Research & Development Projects of China (2016YFA0202300), the MOST (Grant 2013CBA01600), the National Natural Science Foundation of China (Nos. 61390501, 51210003, 11604373, 51572290, and 51325204), and the CAS Pioneer Hundred Talents Program. Work at Vanderbilt University was supported by the U.S. Department of Energy, Grant DE-FG02-09ER46554, and by the McMinn Endowment. Supercomputer time was provided by the National Supercomputer Center in Tianjin and the National Center for Supercomputing Applications. Y.-Y.Z. and S.T.P also acknowledge National Energy Research Scientific Computing Center (NERSC), a DOE Office of Science User Facility supported by the Office of Science of the U.S. Department of Energy under Contract No. DE-AC02-05CH11231, and the Extreme Science and Engineering Discovery Environment (XSEDE), which is supported by National Science Foundation Grant ACI-1053575.

■ REFERENCES

(1) Novoselov, K. S.; Jiang, D.; Schedin, F.; Booth, T. J.; Khotkevich, V. V.; Morozov, S. V.; Geim, A. K. *Proc. Natl. Acad. Sci. U. S. A.* **2005**, *102*, 10451.
(2) Bolotin, K. I.; Sikes, K. J.; Jiang, Z.; Klima, M.; Fudenberg, G.; Hone, J.; Kim, P.; Stormer, H. L. *Solid State Commun.* **2008**, *146*, 351.
(3) Radisavljevic, B.; Radenovic, A.; Brivio, J.; Giacometti, V.; Kis, A. *Nat. Nanotechnol.* **2011**, *6*, 147.

DOI: 10.1021/acs.nanolett.6b04804
Nano Lett. 2017, 17, 1161–1166

(4) Ni, Z. Y.; Liu, Q. H.; Tang, K. C.; Zheng, J. X.; Zhou, J.; Qin, R.; Gao, Z. X.; Yu, D. P.; Lu, J. *Nano Lett.* **2012**, *12*, 113.
(5) Oughaddou, H.; Enriquez, H.; Tchalala, M. R.; Yildirim, H.; Mayne, A. J.; Bendounan, A.; Dujardin, G.; Ait Ali, M.; Kara, A. *Prog. Surf. Sci.* **2015**, *90*, 46.
(6) Tao, L.; Cinquanta, E.; Chiappe, D.; Grazianetti, C.; Fanciulli, M.; Dubey, M.; Molle, A.; Akinwande, D. *Nat. Nanotechnol.* **2015**, *10*, 227.
(7) Zhuang, J. C.; Xu, X.; Feng, H. F.; Li, Z.; Wang, X. L.; Du, Y. *Sci. Bull.* **2015**, *60*, 1551.
(8) De Padova, P.; Kubo, O.; Olivieri, B.; Quaresima, C.; Nakayama, T.; Aono, M.; Le Lay, G. *Nano Lett.* **2012**, *12*, 5500.
(9) Feng, B. J.; Ding, Z. J.; Meng, S.; Yao, Y. G.; He, X. Y.; Cheng, P.; Chen, L.; Wu, K. H. *Nano Lett.* **2012**, *12*, 3507.
(10) Meng, L.; Wang, Y. L.; Zhang, L. Z.; Du, S. X.; Wu, R. T.; Li, L. F.; Zhang, Y.; Li, G.; Zhou, H. T.; Hofer, W. A.; Gao, H. J. *Nano Lett.* **2013**, *13*, 685.
(11) Fleurence, A.; Friedlein, R.; Ozaki, T.; Kawai, H.; Wang, Y.; Yamada-Takamura, Y. *Phys. Rev. Lett.* **2012**, *108*, 245501.
(12) Aizawa, T.; Suehara, S.; Otani, S. *J. Phys. Chem. C* **2014**, *118*, 23049.
(13) Vogt, P.; De Padova, P.; Quaresima, C.; Avila, J.; Frantzeskakis, E.; Asensio, M. C.; Resta, A.; Ealet, B.; Le Lay, G. *Phys. Rev. Lett.* **2012**, *108*, 155501.
(14) Liu, H.; Gao, J.; Zhao, J. *J. Phys. Conf Ser.* **2014**, *491*, 012007.
(15) Kokott, S.; Pflugradt, P.; Matthes, L.; Bechstedt, F. *J. Phys.: Condens. Matter* **2014**, *26*, 185002.
(16) Gao, J. F.; Zhao, J. J. *Sci. Rep.* **2012**, *2*, 00861.
(17) Cahangirov, S.; Ozcelik, V. O.; Xian, L. D.; Avila, J.; Cho, S.; Asensio, M. C.; Ciraci, S.; Rubio, A. *Phys. Rev. B: Condens. Matter Mater. Phys.* **2014**, *90*, 035448.
(18) Bernard, R.; Borensztein, Y.; Cruguel, H.; Lazzeri, M.; Prevot, G. *Phys. Rev. B: Condens. Matter Mater. Phys.* **2015**, *92*, 045415.
(19) Satta, M.; Colonna, S.; Flammini, R.; Cricenti, A.; Ronci, F. *Phys. Rev. Lett.* **2015**, *115*, 026102.
(20) Yi, D.; Jincheng, Z.; Jiaou, W.; Zhi, L.; Hongsheng, L.; Jijun, Z.; Xun, X.; Haifeng, F.; Lan, C.; Kehui, W.; Xiaolin, W.; Xue, D. S. *Sci. Adv.* **2016**, *2*, 1600067.
(21) Fleurence, A.; Friedlein, R.; Ozaki, T.; Kawai, H.; Wang, Y.; Yamada-Takamura, Y. *Phys. Rev. Lett.* **2012**, *108*, 245501.
(22) Sutter, P. W.; Flege, J. I.; Sutter, E. A. *Nat. Mater.* **2008**, *7*, 406.
(23) Pan, Y.; Shi, D. X.; Gao, H. J. *Chin. Phys.* **2007**, *16*, 3151.
(24) Pan, Y.; Zhang, H. G.; Shi, D. X.; Sun, J. T.; Du, S. X.; Liu, F.; Gao, H. J. *Adv. Mater.* **2009**, *21*, 2739.
(25) Zhang, Y. Y.; Mishra, R.; Pennycook, T. J.; Borisevich, A. Y.; Pennycook, S. J.; Pantelides, S. T. *Adv. Mater. Interfaces* **2015**, *2*, 1500344.
(26) Yuan, Y. K.; Quhe, R. G.; Zheng, J. X.; Wang, Y. Y.; Ni, Z. Y.; Shi, J. J.; Lu, J. *Phys. E* **2014**, *58*, 38.
(27) Perdew, J. P.; Burke, K.; Ernzerhof, M. *Phys. Rev. Lett.* **1996**, *77*, 3865.
(28) Kresse, G.; Joubert, D. *Phys. Rev. B: Condens. Matter Mater. Phys.* **1999**, *59*, 1758.
(29) Tersoff, J.; Hamann, D. R. *Phys. Rev. B: Condens. Matter Mater. Phys.* **1985**, *31*, 805.
(30) Kresse, G.; Hafner, J. *Phys. Rev. B: Condens. Matter Mater. Phys.* **1993**, *47*, 558.
(31) Kresse, G.; Hafner, J. *Phys. Rev. B: Condens. Matter Mater. Phys.* **1994**, *49*, 14251.
(32) Cahangirov, A.; Topsakal, M.; Aktürk, E.; Şahin, H.; Ciraci, S. *Phys. Rev. Lett.* **2009**, *102*, 236804.
(33) Ho, K. M.; Fu, C. L.; Harmon, B. N.; Weber, W.; Hamann, D. R. *Phys. Rev. Lett.* **1982**, *49*, 673.

DOI: 10.1021/acs.nanolett.6b04804
Nano Lett. 2017, 17, 1161−1166